

---

# H-mediated magnetic interactions between layers in a two-dimensional Mn-dca polymer: Neutron Diffraction, DFT and Quantum Monte Carlo calculations

Béatrice Gillon,<sup>[a]</sup> Albert Hammerschmied,<sup>[a]</sup> Arsen Gukasov,<sup>[a]</sup> Alain Cousson,<sup>[a]</sup> Thomas Cauchy,<sup>[b]</sup> Eliseo Ruiz,<sup>[c]</sup> John A. Schlueter,<sup>[d]</sup> and Jamie L. Manson<sup>\*,[e]</sup>

Dedication. This paper is dedicated to Olivier Kahn

*[a] Laboratoire Léon Brillouin (LLB), CEA-CNRS, CE Saclay, F-91191 Gif-sur-Yvette Cedex, France; e-mail: [beatrice.gillon@cea.fr](mailto:beatrice.gillon@cea.fr)*

*[b] Université d'Angers, CNRS UMR 6200, Laboratoire MOLTECH-Anjou, 2 bd Lavoisier, 49045 Angers Cedex, France*

*[c] Departament de Química Inorgànica i Orgànica and Institut de Química Teòrica i Computacional, Universitat de Barcelona, Diagonal 645, 08028 Barcelona, Spain*

*[d] Argonne National Laboratory, Materials Science Division, Bldg. 200, 9700 S. Cass Avenue, Argonne, IL 60439 Argonne, USA*

*[e] Department of Chemistry, Biochemistry and Physics, Eastern Washington University, Cheney, WA 99004, USA; e-mail: [jmanson@ewu.edu](mailto:jmanson@ewu.edu)*

**Abstract:** We report neutron diffraction investigations of the quasi two-dimensional  $\text{Mn}(\text{dca})_2(\text{pym})(\text{H}_2\text{O})$  ( $\text{pym} = \text{N}_2\text{C}_4\text{H}_4$ ) compound, where  $\text{Mn}(\text{II})$  ions are bridged by dicyanamide anions,  $[\text{N}(\text{CN})_2]$  (herein abbreviated dca). Inside the layers,  $\text{Mn}(\text{II})$  ions are connected by single or double dca bridges. The magnetic phase diagram was established by neutron diffraction on single crystal. In the low field phase the  $\text{Mn}(\text{II})$  ions are antiferromagnetically ordered in the layers, with moments nearly parallel to the  $\mathbf{c}$  axis and the layers are antiferromagnetically coupled. The spin flop phase corresponds to ferromagnetic coupling between the antiferromagnetic layers, in which the  $\text{Mn}(\text{II})$  moments are nearly perpendicular to the  $\mathbf{c}$  axis. The induced spin density distribution in the paramagnetic phase determined by polarized neutron diffraction visualizes the superexchange pathways through the dca ligands within the layers and through H-bonding between neighboring layers. The theoretical spin density obtained by bidimensional periodic DFT calculations is confronted with the experimental results. Furthermore, quantum Monte Carlo simulations were performed to compare the DFT results with experimental susceptibility measurements.

## Introduction

The dicyanamide anion,  $[\text{N}(\text{CN})_2]$  (herein abbreviated dca), has received much research interest from many scientists around the world over the past years. Long range magnetic order (LRO) was observed in only few of the transition metal containing coordination polymers built with the dca ligand [1-4]. Their detailed characterization using a variety of techniques including powder neutron diffraction and inelastic neutron scattering (INS) permitted to determine magnetic structures, order parameters, and spin dynamics [1-3]. However the superexchange interactions pathways between the transition metal ions in these materials were not yet experimentally characterized. Spin density determination by polarized neutron diffraction (PND) is

particularly suited for such investigations [4-7]. As a matter of fact the mechanism of magnetic coupling between transition metal ions through various bridges (oxamato [5], oxamido [5], di-azido in end-on [6] and end-to-end [7] bridging modes) was clarified with help of this technique [8]. Moreover, the role of H-bonding in magnetic interactions between molecules was evidenced by PND in organic nitroxide radicals [9] [10].

One of the most thoroughly investigated family of dca-based materials is the rutile-like  $\text{M}(\text{dca})_2$  series, which forms a 3D-network of  $\text{M}_{2+}$  ions connected by dca bridges in  $\mu_3$ -coordination mode, i.e. each N of the dca ligand is connected to one M [1]. Other compounds involving another type of ligand beside dca, like  $\text{Mn}(\text{dca})_2\text{-pym}$  [2],  $\text{Mn}(\text{dca})_2\text{-o-phen}$  [3],  $\text{Mn}(\text{dca})_2\text{pym}_2$  and  $\text{Mn}(\text{dca})_2(\text{pym})(\text{H}_2\text{O})$  ( $\text{pym} = \text{pyrimidine} = \text{N}_2\text{C}_4\text{H}_4$ ) [4] present  $\mu_{1.5}$ -coordination mode for dca bridging, i.e. only the terminal N atoms of dca are connected to M ions, and form low dimensional structures which present antiferromagnetic LRO at low temperature.

In this paper we report detailed neutron diffraction investigations of the magnetism in the quasi 2-dimensional compound  $\text{Mn}(\text{dca})_2(\text{pym})(\text{H}_2\text{O})$ . This compound [4] consists of a quasi 2D-network with two types of dca bridges, i.e. single ( $\text{Mn-NCNCN-Mn}$ ) and double ( $\text{Mn-(NCNCN)}_2\text{-Mn}$ ) bridges alternately arranged within the layer. Layers are held together via hydrogen bonding between coordinated  $\text{H}_2\text{O}$  ligands and nitrogen atoms of the pyrimidine ring or amide nitrogen atoms from dca. From single crystal ac susceptibility measurements, a collinear antiferromagnetic ordering in zero magnetic field at low temperature was observed below 2.4 K as well as a spin flop transition induced by the application of an external field of 1.2 T at 1.7K along the  $\mathbf{c}$  axis [4].

In the first part, the determination of the low temperature magnetic structures, in zero field and under an applied magnetic field, is described. In the second part, the spin density maps determined by polarized neutron diffraction (PND) in the induced paramagnetic phase are reported. The nature of the magnetic interactions and the superexchange pathways are discussed in the light of the experimental and theoretical results.

## Results and discussion

### Low temperature nuclear structure

According to X-ray diffraction at 173 K [4],  $\text{Mn}(\text{dca})_2(\text{pym})(\text{H}_2\text{O})$  crystallizes in the  $P2_1/c$  monoclinic space group with cell parameters  $a = 7.3939(17)$  Å,  $b = 18.858(4)$  Å,  $c = 8.849(2)$  Å and  $\beta = 109.260(4)$  degrees. The neutron structure determination at

30K was carried out using the CRYSTALS software [11]. Initial atomic positions were taken from the earlier X-ray structure determination at 173 K. The least-squares refinement of the scale factor, the extinction parameter, the atomic coordinates and anisotropic temperature factors for all atoms resulted in a final agreement factor of  $R(F_N) = 0.042$  and goodness of fit  $GOF = 1.046$  for 1731 independent reflections with  $I_o > 3\sigma(I_o)$ . A value of 4.6(3) was obtained for the refined extinction parameter [12]. The corresponding extinction corrections on the nuclear structure factors  $F_N$  were not exceeding 20 per cent for the most intense reflections and therefore extinction was neglected in further treatment. The structural parameters are listed in Supplementary Information. The dca bridged  $Mn_{II}$  ions form layers parallel to the  $(2\mathbf{a}+\mathbf{c}, \mathbf{b})$  plane, as represented in Figure 1a, in projection along the  $(2\mathbf{a}+\mathbf{c})$  direction. Inside each layer, the  $Mn_{II}$  ion in  $(x, y, z)$  position is related by single dca bridges to two manganese atoms in  $(x, \frac{1}{2} - y, \frac{1}{2} + z)$  and  $(x - 1, \frac{1}{2} - y, z - \frac{1}{2})$  positions and to one manganese atom in  $(-x, 1 - y, 1 - z)$  position by a double dca bridge as shown in Figure 1b in projection along the  $\mathbf{b}$  axis. The Figure 2 shows the stacking of the layers along the  $\mathbf{c}$  axis with two types of hydrogen bonds  $N8..H2O1$  and  $N4..H1O1$  connecting the neighboring layers ( $N..H$  distances shorter than  $2.0 \text{ \AA}$ ).

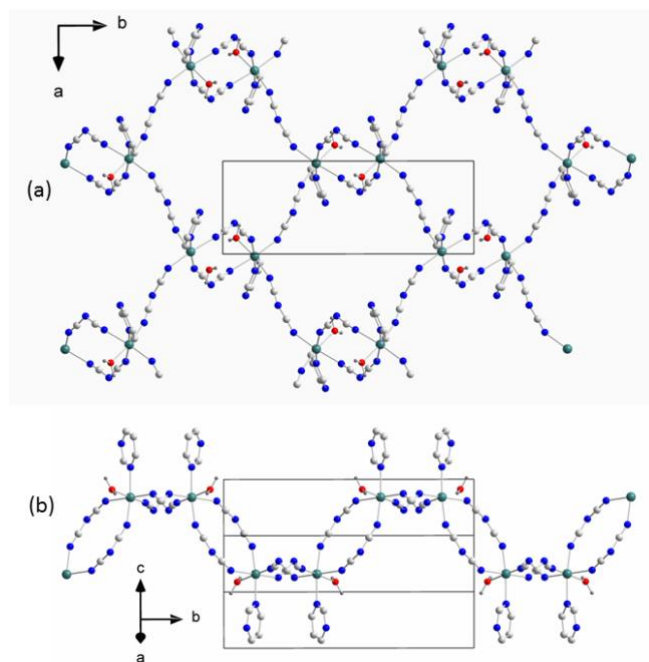


**Figure 1.** View of one layer (a): in projection along the  $\mathbf{c}$  direction; (b) down the  $(2\mathbf{a} + \mathbf{c})$  direction

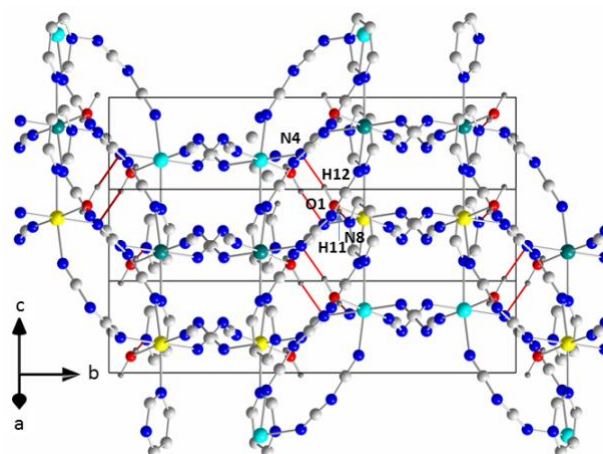


**Figure 2.** Bidimensional structure of the  $Mn(dca)_2pymH_2O$  compound: stacking of the layers along the  $\mathbf{c}$ -axis, viewed down the  $(2\mathbf{a} + \mathbf{c})$  direction; H-bonds between neighboring layers  $O1H12\dots N4$  and  $O1H11\dots N8$  are indicated in red lines.

The main interatomic distances obtained from neutron diffraction on single crystal at 30K, inside and between the layers, are reported in Table 1 together with the X-ray values at 173K. A significant shortening of the hydrogen bonds, of 7 per cent for  $N8H2$  and 9 per cent for  $N4H1$ , is observed between 173 and 30K while all other bonds remain constant.

**Table 1.** Main intra- and inter-layer distances at 173 and 30K. Interlayer H bonds relate  $H_2O$  linked to  $Mn(x,y,z)$  of one layer to the double dca bridge ( $N4$ ) and to the pym ring ( $N8$ ) of the neighboring layer.

Bond length	T = 173K (X-rays)	T = 30K (this work)
MnN1	2.187(1)	2.174
MnN3	2.202(1)	2.201
MnN4	2.268(1)	2.260
MnN6	2.202(1)	2.236
MnN7	2.290(1)	2.328
MnO1	2.191(1)	2.195
$N8\dots H1$	1.932	1.757
$N4\dots H2$	2.126	1.986

### Magnetic phase diagram and magnetic structures

Antiferromagnetic peaks of  $(h + \frac{1}{2}, k, l)$  type were observed by neutron diffraction on single crystal at 1.5K in zero magnetic field due to the onset of the low temperature antiferromagnetic ordering, denoted AF1. The temperature-dependence of the  $(-\frac{1}{2}, 3, 0)$  antiferromagnetic reflection is reported in Figure 3a. The intensity of this peak decreases when temperature increases and

reaches zero at 3K which provides a precise estimation of the ordering temperature  $T_N$ . No difference between the  $(h, k, l)$  nuclear peaks intensities at 4.3K and 1.5K was found.

The Figure 3b displays the field dependence of the peak intensity of the  $(\frac{1}{2}, 3, 1)$  antiferromagnetic reflection at 2.6 K. The intensity drops to zero when the field is increased above 0.95 T. Under a field larger than 0.95 T, the antiferromagnetic peaks  $(h + \frac{1}{2}, k, l)$  disappear and no other type of antiferromagnetic peaks is observed. In the meanwhile, some magnetic intensity appears on the  $(h, k, l)$  peaks as evidenced in Figure 3b by the field-dependence of the  $(1, 0, 1)$  reflection at 2.6 K. This particular reflection has been chosen as it has a very low nuclear scattering contribution. This means that another antiferromagnetic state, denoted AF2, occurs above  $H_{c1} = 0.95$  T at 2.6 K, with a propagation vector  $k = 0$ . Further increase of the magnetic field induces a canting of the antiferromagnetically coupled moments towards the field direction, reflected by the decrease of the intensity of the  $(1, 0, 1)$  reflection.

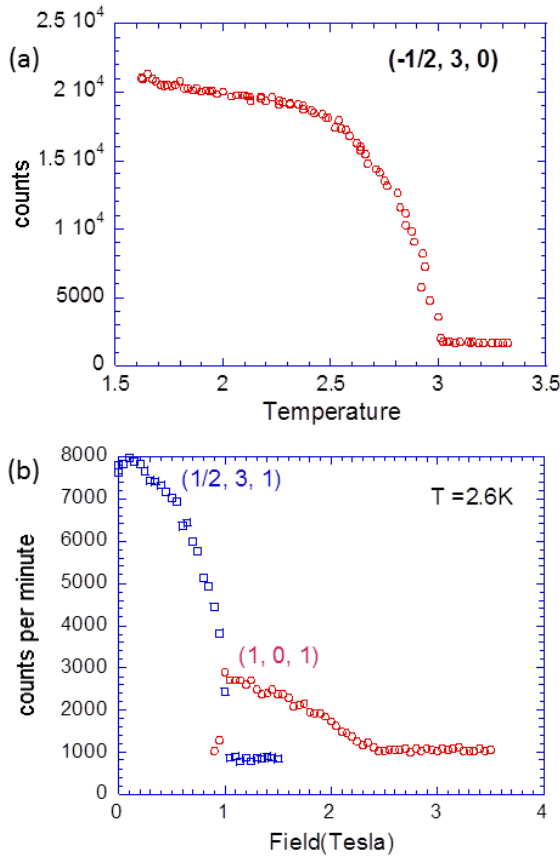


**Figure 3.** Integrated intensities of some antiferromagnetic peaks observed by neutron diffraction: a) Variation of the  $(-\frac{1}{2}, 3, 0)$  antiferromagnetic peak intensity versus temperature in zero field; b) Variation of the  $(\frac{1}{2}, 3, 1)$  antiferromagnetic peak intensity versus magnetic field.

The magnetic phase diagram in Figure 4 was established by measuring the field dependence of the  $(\frac{1}{2}, 3, 1)$  and  $(1, 0, 1)$  peaks at various temperatures, showing the domain of existence of the (low temperature, low field) AF1 antiferromagnetic structure and the spin flop AF2 antiferromagnetic structure.

Neutron diffraction provides a value of  $T_N = 3$  K for the Neel temperature of the zero-field AF structure while this temperature was estimated to 2.4K due to the existence of a sharp peak in the plot of  $d(\chi.T)/dT$  versus  $T$ . However a broad maximum of the magnetic susceptibility was observed at 2.95K on the  $\chi(T)$  curve measured on single crystal with a field applied along the  $c$  axis (see Fig. 8 of reference [4]) that was attributed to short range magnetic coupling in the layers. The observation of magnetic reflections just below 3K shows that long range magnetic ordering indeed already takes place. The spin flop transition field  $H_{c1}$  (0.95 Tesla) observed at 1.5K by neutron diffraction is weaker than the value of 1.56 Tesla deduced from the magnetic susceptibility measurements at 1.7K [4]. This discrepancy could be due to a misalignment of the  $c$  direction of the crystal with the field on the SQUID. If the field is not exactly applied along the  $c$  axis, higher magnetic fields are required at a given temperature (1.7K) to induce the spin flop transition at  $H_{c1}$  (1.56T) and the aligned paramagnetic state at  $H_{c2}$  ( $>4.5$ T) compared to  $H_{c1}=0.9$ T and  $H_{c2}=3.2$ T deduced from neutron diffraction (1.5K).

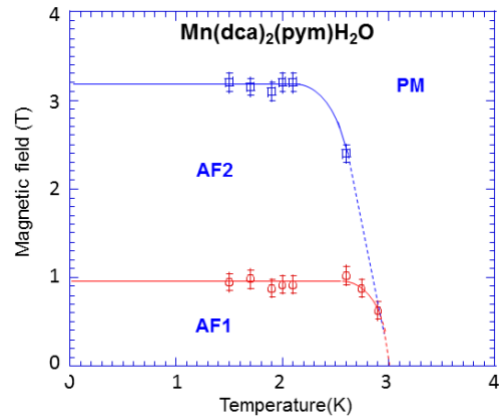


**Figure 4.** Experimental magnetic phase diagram of  $Mn(dca)_2(pym)H_2O$  from neutron diffraction on single crystal.

The AF1 structure was determined by refinement based on the magnetic structure factors given by the square roots  $|F_M| = I_{AF}^{1/2}$  of the observed intensities of  $(h + \frac{1}{2}, k, l)$  reflections at 1.5K. It leads to an antiferromagnetic structure with propagation vector  $(\frac{1}{2}, 0, 0)$  and with moments of the four  $Mn_{II}$  ions of each nuclear cell parallel to each other and antiparallel to those of the neighboring cell in the  $a$  direction. A weighted agreement factor  $R_w(|F_M|) = 0.074$  and a goodness of fit of 1.87 were obtained for the refinement based on 57 observed magnetic reflections. In the low field AF1 phase displayed in Figure 5, the  $Mn_{II}$  moments are antiferromagnetically coupled in the layers (through single and double  $dca$  bridges) and oriented at 11 degrees from the  $c$  axis in the  $(a, c)$  plane. The

neighboring layers, connected through H bonding (N8..H1O1 and N4..H2O1), are antiferromagnetically coupled.

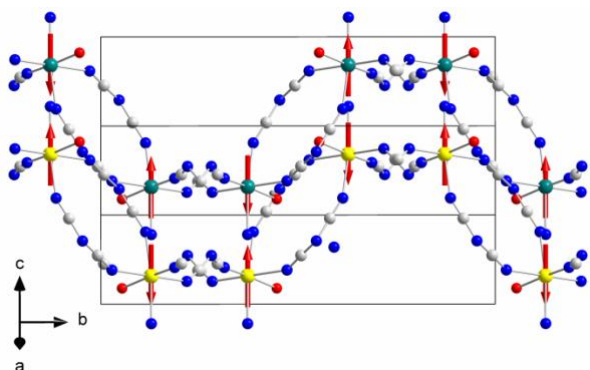


**Figure 5.** Zero field AF1 magnetic structure at 1.5K in projection along the (2a+c) direction. The magnetic moment directions are nearly parallel to the c axis, at 11 degrees from the c axis in the (a,c) plane. Mn atoms belonging to two different layers are represented in green and yellow respectively.

The magnetic intensities at 1.5 K were obtained by difference between the intensities of the (h,k,l) reflections measured under 1.2 Tesla and zero field. The magnetic structure was obtained by refinement on the basis on 50 reflections with agreement factors  $R_w(|F_M|) = 0.021$  and  $GOF = 2.97$ . In the field-induced AF2 phase ( $H \parallel c$ ) represented in Figure 6, the four  $Mn_{II}$  ions in the unit cell carry antiferromagnetic moments nearly perpendicular to the direction (the angle is 101 degrees with respect to c). The  $Mn_{II}$  moments are antiferromagnetically ordered inside the layers (like in the low field AF1 phase), but ferromagnetically coupled with the two neighboring layers. In this phase, the direction of the induced moments flip by 90° from the previous direction in zero-field i.e. become nearly perpendicular to the applied field. The intralayer coupling remains antiferromagnetic but the interlayer coupling becomes ferromagnetic. A magnetic field  $H_{c1} < H < H_{c2}$  overcomes the antiferromagnetic interaction between the layers but not inside the layers. This shows that the intralayer antiferromagnetic coupling is stronger than the antiferromagnetic coupling between the layers. Above  $H_{c2}$ , the intralayer antiferromagnetic interactions are overcome and all Mn moments are aligned along the field direction c.

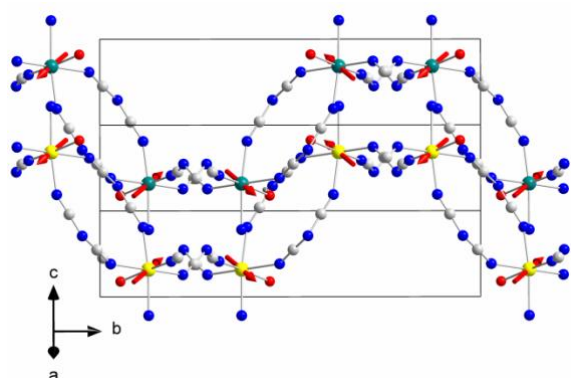


**Figure 6.** Field-induced AF2 antiferromagnetic structure at 1.5K under a field of 1.2 T applied along the c axis, viewed in projection along (2a+c): the magnetic moments are nearly perpendicular to the c axis and contained in the (a,b) plane. Neighboring layers are ferromagnetically coupled (Mn atoms in yellow and green respectively).

### Induced spin density maps in the paramagnetic state at 5K and 10K.

The PND technique gives access to the induced magnetic structure factors  $F_M$  with high precision and therefore enables to retrieve detailed spin density maps in the induced paramagnetic state of molecular compounds [4-7]. It consists in measuring the flipping ratios  $R(hkl)$  of the Bragg reflections, i.e. the ratio between the diffracted intensities  $I_+$  and  $I_-$  corresponding to opposite directions of the vertical polarization of the incident beam.

$$R(hkl) = \frac{I_+}{I_-} = \frac{|F_N + F_M|^2}{|F_N - F_M|^2} \quad (1)$$

where  $F_N$  is the nuclear structure factor corresponding to the low temperature nuclear structure which is determined by a complementary neutron diffraction experiment. Applying a magnetic field of 4.5 T along the easy axis c above  $T_N$  permits to align all magnetic moments in the sample along the field. Therefore it is justified to apply the classical spin density model refinement [8] to analyze the PND data. The spin density was reconstructed by model refinement on the flipping ratios [13] using the  $F_N$  values calculated from the neutron structure at 30 K. A correction was introduced for the contribution due to the nuclear polarization of the H nuclei at low temperature by a high magnetic field.

A multipole model describing the spin density was refined on the basis of the observed flipping ratios. For the data analysis at 5K, a scale factor was refined in order to take into account the existence of two independent data collections on 5C1 and 6T2 (see Exp Section - Table 6) and a value of 0.996(17) was obtained, i.e. very close to 1. This confirms the excellent agreement between the two data collections performed on two different single crystals on two different diffractometers at two different wavelengths. The model assumes spherical densities on all atoms including the H atoms of  $H_2O$ . As a matter of fact the spin density for a 3d<sup>5</sup> ion like  $Mn_{II}$  ( $S = 5/2$ ) is expected to be spherical. In this model, the spin density is written as the sum of independent atomic densities described by a Slater type radial function:

$$\rho(r) = \sum_i P_{00}^i N r^{n_i} e^{-\kappa_i \zeta_i r} \quad (2)$$

where  $P_{00}^i$  is the monopole population, N is a normalization factor,  $\zeta_i$  is a Slater-type exponent and  $\kappa_i$  is a contraction coefficient which can be refined. The radial exponents  $\zeta_i$  reported in Table 2a were taken from literature [14] and only the contraction coefficient  $\kappa_i$  of the manganese atom was refined. A step by step procedure was followed for the model refinement: the Mn monopole and its radial expansion were first refined, then the monopoles of the Mn's first, second and following neighbors were introduced stepwise in the refinement. The obtained monopole populations provide the



experimental values of the induced magnetic moments on each atom in the cell.

**Table 2a.** Radial functions parameters used in the spin density multipole model

atom	n	radial exponents (ua <sup>-1</sup> ) [a]
Mn	4	7.02
N	2	3.90
C	2	3.44
O	2	4.45
H	1	2.48

[a] exponents are equal to twice the values of the orbital Slater exponent given in [14]

Table 2b displays the obtained magnetic moments from least squares refinement at 10K and 5K. At each step, the refined populations which were smaller than twice the error bar were set to zero in further refinements and are not reported in Table 2b. The sum of the magnetic moments over a Mn(dca)<sub>2</sub>pym(H<sub>2</sub>O) unit provides an estimation of the induced magnetization in the conditions of temperature and field: 3.06(7)  $\mu_B$  at 5K and 2.06(7)  $\mu_B$  at 10K under a field of 4.5 T applied along the **c** axis. The spin distributions obtained at 10K and 5K are in qualitative agreement, however a more detailed spin distribution is obtained at 5K. Therefore we discuss in this paper the spin density maps obtained from model refinement at 5K only, which are displayed in Figures 7 to 9. Only the populations larger than twice the error bar were taken into account for the spin density reconstruction. The distribution of the spin density over the Mn<sup>II</sup> ions and the ligands permits to visualize the magnetic interaction pathways in the paramagnetic phase.

**Table 2b.** Induced atomic magnetic moments P (in  $\mu_B$ ) at 5K and 10K under 4.5T from spin density model refinement on the basis of the experimental flipping ratios and refinement conditions. Only atoms with populations larger than 2 $\sigma$  are listed.

atom	P(5K)	P(10K)
Mn	2.82(3)	1.88(2)
N1	0.08(1)	0.05(1)
N4	0.04(1)	0.05(2)
C2	0.03(1)	0.02(1)
C4	-0.05(1)	-0.03(1)

N7	0.04(1)	0
N8	0.08(2)	0.05(2)
C5	-0.09(2)	-0.05(2)
H2	0.03(1)	0
N observations ( $ 1-R >3\sigma$ )	185	120
N parameters	11	8
GOF	5.5	4.2
Rw( $ 1-R $ )	0.08	0.09

The projection of the spin density onto the plane of the single dca bridge is drawn in Figure 7. The Figure 8 illustrates the spin distribution on the double dca bridge, which is connected to the H2 atom belonging to the water molecule of the neighboring layer by an hydrogen bond N4..H2O1. This map was obtained by integration along the direction perpendicular to the (MnN4H2) plane.

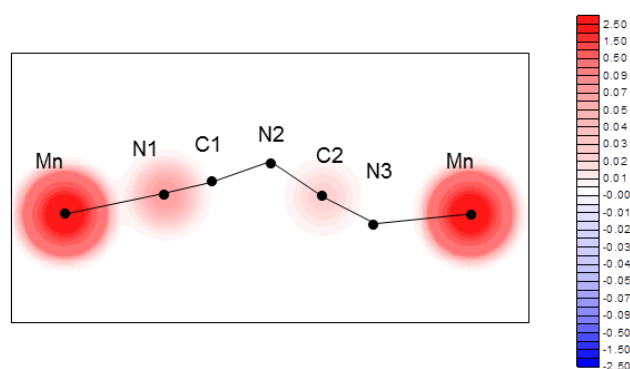


**Figure 7.** Projection of the spin density from model refinement at 5K onto the Mn-N1C1-N2-C2N3-Mn single dca bridge plane (in  $\mu_B \cdot \text{\AA}^{-2}$ ).

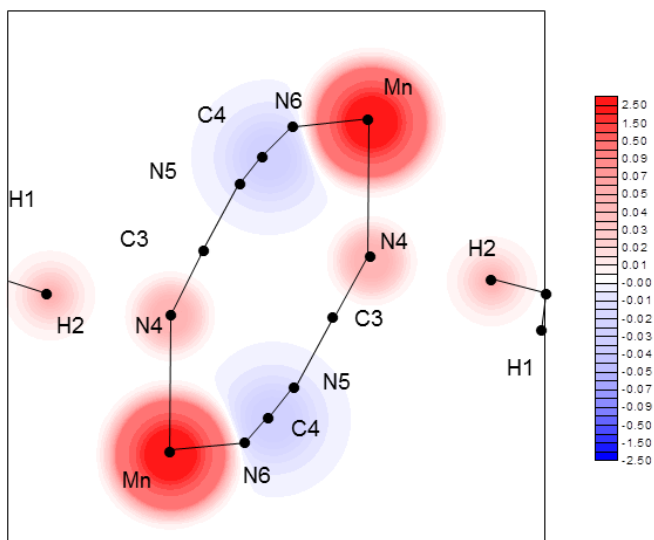


**Figure 8.** Spin density map at 5K for the double dca bridge in projection along the perpendicular to the MnN4H2 plane: visualization of the interlayer N4...H2-O1 hydrogen bond (in  $\mu_B \cdot \text{\AA}^{-2}$ ).

On the single dca bridge, a positive spin density is observed on one terminal nitrogen atom (N1) together with a very weak positive population on one C atom (C2). On the double dca bridge, a positive spin density is also present on one terminal nitrogen atom (N4), while a negative spin density lies on the carbon atom (C4) which reflects a spin polarization effect of the dca group due to the  $Mn_{III}$  ion. The spin transfer from the Mn atom towards the dca ligands is responsible for the overlap between the magnetic orbitals centered on two neighboring Mn in the layers and therefore favors an antiferromagnetic coupling between neighboring Mn ions inside the layer [15].

A small positive spin density is observed on the H2 atom involved in the N4...H2O1 bond at the same time as the positive spin density on N4 (Figure 8). This evidences the possible interaction pathway for the magnetic coupling between neighboring layers. The existence of the positive spin population on this hydrogen atom is crucial for understanding the establishment of the interlayer antiferromagnetic interactions. A positive spin density on H atom was previously evidenced by PND in induced paramagnetic phases in the tempol nitroxide radical [9] which orders antiferromagnetically and a nitronyl nitroxide radical [10] which forms ferromagnetic chains. In both cases a depletion of the spin density localized on the O atom of the nitroxide NO group was observed together with a positive spin transfer towards the H involved in the O...HC bond.

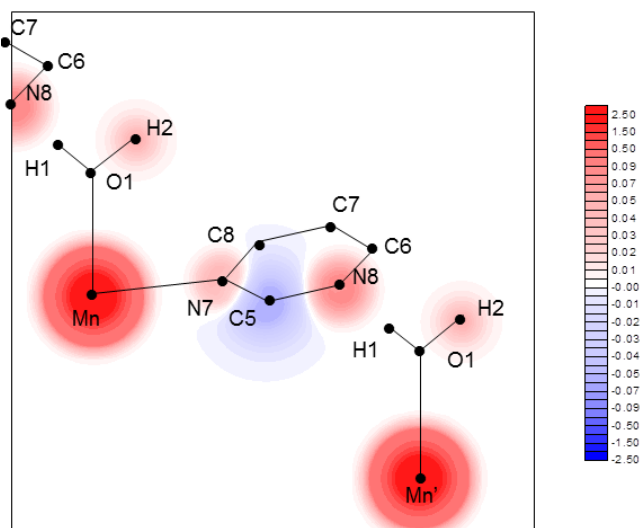


**Figure 9.** Spin density map at 5K for the pym and H<sub>2</sub>O ligands, in projection along the perpendicular to the O1H1N8 plane: visualization of the interlayer N8...H1-O1 hydrogen bond (in  $\mu_B \cdot \text{\AA}^{-2}$ ).

The spin distribution on the pyrimidine ring is displayed in Figure 9, showing the connection between the pyrimidine ring and the water molecule of the neighboring layer through the N8...H1O1 hydrogen bond. The map in Figure 9 was obtained by integration of the spin density along the direction perpendicular to the (N8O1H1) plane. The nitrogen atom N7 of the pyrimidine ring coordinated to Manganese carries a positive spin density of the same order of magnitude as the N1 and N4 atoms of the dca bridges and can be attributed to a spin delocalization effect. The C8 carbon atom in ortho position carries a negative spin density, while the N8 atom in meta carries a positive spin density. The alternation of signs of the spin density on the ring suggests the existence of  $\pi$ - $\pi$  spin polarization.

### DFT calculations

For a periodic system, the Heisenberg Hamiltonian must include the existence of several exchange pathways with different J values. A detailed discussion of the calculation of the exchange coupling constants in periodic systems can be found in ref. [16]. If one neglects spin-orbit coupling effects, the Hamiltonian for a general extended structure is indicated in Eq. (3):

$$\hat{H} = -\sum_{i>j} J_{ij} \hat{S}_i \hat{S}_j \quad (3)$$

where  $\hat{S}_i$  and  $\hat{S}_j$  are the spin operators of the different paramagnetic centers. The J values are the coupling constants between all the paramagnetic centers. The periodicity of the structure allows us to restrict ourselves to interactions within a single unit cell. Thus, for the  $Mn(dca)_2(pym)(H_2O)$  compound we can define two exchange coupling constants  $J_1$  and  $J_2$  corresponding to the single and double dicyanamide bridges, respectively (see Figure 10):

$$\hat{H} = J_1(\hat{S}_1\hat{S}_2 + \hat{S}_3\hat{S}_4) + J_2(\hat{S}_2\hat{S}_3 + \hat{S}_4\hat{S}_1) \quad (4)$$

The procedure employed by us here for the estimation of the set of exchange coupling constants in an extended compound with  $n$  different  $J_{ij}$  values consists in the calculation of  $(n+1)$  energies corresponding to different spin distributions within the unit cell. It is similar that employed for molecular polynuclear complexes [17, 18] but restricted to the unit cell. We can use such energies to obtain a system of  $n$  equations with  $n$  unknowns, the  $J_{ij}$  values. Thus, we have calculated three energies, the high spin solution with all the manganese atoms with spin up and two spin distributions with  $S = 0$  with the inversion of the spin of two manganese atoms (Mn2, Mn3 and Mn2, Mn4 respectively).

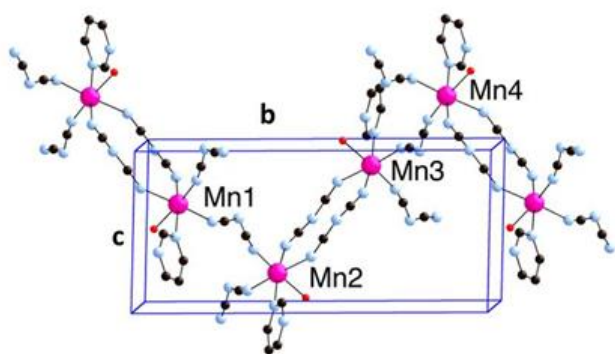


**Figure 10.** Structure of the bidimensional system of the  $\text{Mn}(\text{dca})_2(\text{pym})(\text{H}_2\text{O})$  considered in the periodic calculations.

The use of some hybrid exchange-correlation functionals provides an accurate description of the exchange interactions in polynuclear transition metal systems.[19-21] Hence, two different types of calculations were performed: first, with the periodic algorithm implemented in the Gaussian03 code[22] using the B3LYP functional[23] using 216  $k$ -points in the irreducible part of the first Brillouin zone while 221 neighbor cells were considered for the estimation of the contribution energy terms. We have employed a triple- $\zeta$  basis set for Mn[24] while for the other elements a double- $\zeta$  basis set was used.[25] The more diffuse  $s$  function of the Mn atom was removed and the exponent of the next one was slightly modified. The guess functions were generated with the Jaguar 6.0 code[26] using a molecular model of the unit cell and subsequently, they were employed in the periodic calculations with the Gaussian03 code. The calculations with molecular models were performed with Gaussian03 code using the same functional and basis sets. A second theoretical approach, using the all electron code fhi-aims[27] using high quality numerical functions (tight basis set and a reciprocal grid with 4  $k$ -points) was also employed combined with B3LYP functional. The treatment of the periodic structure is slightly different than the approach implemented in Gaussian03. This computer code is particularly efficient for the study of magnetic properties of very large discrete systems or periodic structures.[28,29]

The calculated  $J_1$  and  $J_2$  values obtained for a bidimensional model of the studied compound are indicated in Table 3. First of all, we note that the two employed theoretical approaches provide qualitatively similar results: the two exchange coupling constants show weak antiferromagnetic values in agreement with the SQUID experimental data[4]. However, only the results with the fhi-aims code show that the presence of a double bridge enhances the strength of the coupling in comparison with the simple bridge, as proposed experimentally[4]. It is worth noting that the coupling through the 1,5 coordinated dicyanamides has a similar sign and strength to that obtained when for the 1,3 coordination mode despite the longest exchange pathway.

**Table 3.** Description of the bridging ligands, Mn...Mn distances (in Å) and DFT calculated and experimental exchange coupling constants  $J$  (in  $\text{cm}^{-1}$ ).

Coupling constant	bridging ligands	d(Mn...Mn)	$J$ ( $\text{cm}^{-1}$ )		
			Gaussian03	fhi-aims	Exp[4]
$J_1$	$\text{N}(\text{CN})_2$	8.60	-0.6	-0.5	-0.14
$J_2$	$[\text{N}(\text{CN})_2]_2$	7.66	-0.7	-1.1	-0.30

To perform a comparison with the experimental magnetic data[4], quantum Monte Carlo (QMC) simulations have been performed for a 2D layer system were based on the directed loop algorithm method developed by Sandvik et al.[30] were carried out using the ALPS 2.0 library (dirloop\_sse method).[31] For the susceptibility dependence with the temperature, usually we employ  $10^8$  steps for the simulations between 2 and 300 K and a whole simulation must be performed at each temperature. The initial 10% of steps was employed for thermalization of the system in all calculations. This kind of simulations allows to properly handle periodic systems that cannot be treated with exact diagonalization methods.

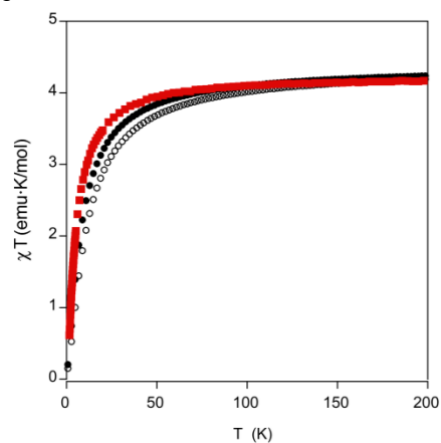


**Figure 11.** Quantum Monte Carlo simulations of the  $\chi \cdot T$  curves using the DFT  $J$  values (see Table 3). Filled and empty circles for Gaussian03 and fhi-aims results, respectively. Squares are the experimental susceptibility data.

The QMC results using the two sets of DFT J values are presented in Figure 11, DFT results nicely reproduce the experimental data. However, the DFT J values slightly overestimate the antiferromagnetic character[4] resulting in a too fast decay of the  $\chi$ :T product at low temperatures.

In order to check the exchange coupling interactions through hydrogen bond interactions between layers, we have performed the calculations with a molecular model shown in Fig. 12. The calculated  $J_3$  value for the interaction between two  $Mn_{II}$  cations at 5.63 Å is  $-0.08 \text{ cm}^{-1}$ . The same value was obtained with the fhi-aims code adding a third  $J_3$  value in the unit cell. This small  $J_3$  value confirms that the coupling between the layers is very weak. The larger theoretical values of the intralayer coupling constants  $J_1$  and  $J_2$  (around  $1 \text{ cm}^{-1}$ ) compared to the interlayer coupling constant  $J_3$ , that is one order of magnitude smaller, are in agreement with the experimental results from neutron diffraction. Such experimental data indicates that the intralayer antiferromagnetic coupling through single or double dca bridges inside the layers is stronger than the antiferromagnetic coupling between the layers.

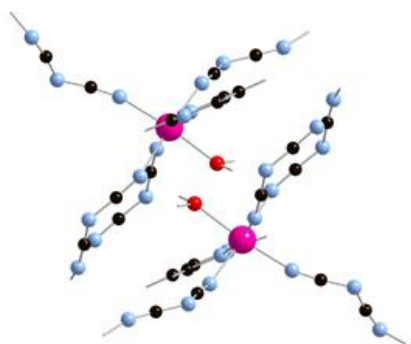


**Figure 12.** Molecular model employed to study the exchange interactions between layers.

The calculated Mulliken spin populations are reported in Table 4. A weak delocalization of the spin density of the  $Mn_{II}$  cations towards the ligands is predicted by calculations, as expected due to the large number of unpaired electrons. [32,33]. The theoretical spin distributions on the single and double dca bridges are similar: the terminal nitrogen atoms directly bonded to Mn carry negative populations while positive spin populations reside on the carbon atoms and the central nitrogen atom. A slight dissymmetry between the spin populations of the two CN groups may be noticed inside the single dca bridge (C1N1 and C2N3) while they are symmetrical in the double dca bridge (C3N4 and C4N6). On the pyrimidine ring, a weak positive spin population is predicted on N7, linked to Mn. The spin distribution on the ring shows positive populations on the C atoms in ortho and para positions and negative populations on the C and N atoms in meta positions.

Weak positive spin populations are also predicted on the O and H atoms of the  $H_2O$  ligand.

**Table 4.** Atomic spin populations (in  $e^-$ ) from periodic DFT calculations (Gaussian03 values and in parenthesis those with fhi-aims code) and from PND at 5K and 10K under 4.5 Tesla, after normalization to 5 unpaired electrons.

	atom	DFT	Experimental (5K)	Experimental (10K)
	Mn	4.832 (4.795)	4.72(5)	4.77(6)
dca (single)	N1	-0.009 (-0.005)	0.13(2)	0.12(4)
	C1	0.035 (0.025)	0	0
	N2	0.016 (0.011)	0	0
	C2	0.027 (0.032)	0.06(2)	0.06(3)
	N3	-0.002 (-0.002)	0	0
dca (double)	N4	-0.001 (0.001)	0.07(2)	0.13(4)
	C3	0.023 (0.021)	0	0
	N5	0.012 (0.009)	0	0
	C4	0.025 (0.031)	-0.08(2)	-0.08(4)
	N6	-0.002 (-0.001)	0	0
pyrimidine	N7	0.010 (-0.022)	0.07 (2)	0
	C5	0.005 (0.022)	-0.15(3)	-0.13(4)
	N8	-0.001 (-0.091)	0.06(2)	0.12(5)
	C6	0.004 (0.030)	0	0
	C7	-0.002 (-0.170)	0	0
	C8	0.005 (-0.074)	0	0
water	O1	0.007 (0.005)	0	0
	H1	0.006 (0.413)	0	0
	H2	0.009 (0.05)	0.06 (2)	0

The experimental spin populations obtained from the induced magnetic moments after normalization to 5 unpaired electrons are reported in Table 4 for comparison with the calculations. It has to be noticed that the experimental spin populations obtained at 5K and 10K are in very good agreement, proving that the 5K results are not biased by short range antiferromagnetic interactions above  $T_N$  (3K).

The predicted amount of spin transfer from  $Mn_{II}$  towards the ligands is in agreement with experiment as shown by the theoretical Mn spin population around 4.8  $e^-$  compared to the experiment value of 4.72(5)  $e^-$ . However, some discrepancies between the theoretical and experimental spin distributions on the ligands can be noticed. Firstly, the theoretical spin populations of the terminal N atoms of the dca bridges have an opposite sign



compared to the observed ones on N1 (single bridge) and N4 (double bridge). Secondly, only one terminal N atom of both single and double dca bridges carry some population, while a symmetrical distribution on the two CN groups was predicted from calculations.

The N7 atom of the pyrimidine ring, linked to the Mn atom, carries a positive spin population in one of the DFT methods, in agreement with observation. However opposite signs are predicted for the spin populations of the C5 and N8 atoms of the ring compared to the observed values. Another discrepancy between theory and experiment lies in the asymmetric distribution of the experimental spin density on the pym ring on both sides of a N7-C6 direction. As a matter of fact, spin densities are observed on one side only of the pyrimidine ring, the side which is involved in the N8...H1O1 bond. Although no spin density was observed on H1 in the limit of experimental accuracy, the dissymmetry of the spin distribution on the pym ring may be due the effect of H-bonding on the spin distribution on the pyrimidine ring. Therefore H1-bond could also play a role in the interlayer magnetic coupling. The large spin density obtained with fhi-aims in the water molecule could be due to an artifact due to the use of a numerical basis set. It has to be noticed that a weak positive spin population is predicted on both H atoms of the H<sub>2</sub>O molecule, larger for H2 than for H1, in agreement with the significant population observed by PND on the H2 atom only.

## Conclusions

The magnetic phase diagram of the quasi bidimensional Mn(dca)<sub>2</sub>(pym)(H<sub>2</sub>O) compound was established by neutron diffraction on single crystal. The low temperature antiferromagnetic structures in the low field phase and in the spin flop phase were determined. The magnetic interaction pathways within and between the layers were given into evidence on the induced spin density maps measured in the paramagnetic phase under high magnetic field.

In the layers the dca single and double bridges favor antiferromagnetic coupling between the Mn atoms due to the overlap between the magnetic orbitals of the system formed by each Mn and its ligands. The two DFT approaches confirm such result indicating that the two different exchange interactions are weak and antiferromagnetic. Quantum Monte Carlo simulations to calculate the susceptibility curves using the DFT J values are in nice agreement with the experimental data.

The interlayer interaction is weaker than the intralayer antiferromagnetic interactions due to dca bridges, as it is overcome by the application of a magnetic field H<sub>c1</sub> while the intralayer AF coupling is retained. The magnetic interaction pathway through H-bonding between the layers is confirmed by the observation by PND of a positive spin density on one H atom of the water molecule involved in an H-bond with the double dca bridge and also by the dissymmetry of the spin distribution on the pym ring involved in H-bonding with the other H atom.

DFT calculations of the spin density in Mn(dca)<sub>2</sub>(pym)(H<sub>2</sub>O) for a bidimensional periodic model quantitatively predict the spin transfer from the Mn<sup>II</sup> ions towards the ligands but provide

opposite signs for the spin populations on the nitrogen atoms of the dca groups. Such prediction indicates that spin polarization is predominant over spin delocalization for the nitrogen atoms of the dca ligand directly coordinated to the Mn<sup>II</sup> centers. This trend is unexpected but the long Mn-N distances make that the spin delocalization due to the metal-ligand orbital mixing is small.[32] The positive spin populations predicted by DFT calculations on the H atoms of the water molecule are in qualitative agreement with the observed one H atom and confirm the possible magnetic pathway through H-bonding for the antiferromagnetic coupling between the layers.

## Experimental Section

**Synthesis.** Synthesis of partially deuterated Mn(dca)<sub>2</sub>(pym)(H<sub>2</sub>O) was performed using deuterated pyrimidine (N<sub>2</sub>C<sub>4</sub>D<sub>4</sub>) following the protocol described in reference [3]. Large single crystals of around 100 mm<sup>3</sup> were obtained by slow evaporation.

**Low temperature structural study by neutron diffraction.** A data collection was performed on the 4-circle neutron diffractometer 5C2 at LLB-Orphée (Saclay, France) in order to determine the nuclear structure at low temperature, which is necessary for the treatment of the PND data. The details about this data collection are reported in Table 5. A large single crystal of size (9 × 4 × 3.5) mm<sup>3</sup> was set in a He-flow cryostat and cooled down to 30K. The wavelength was 0.833 Å. The cell parameters at 30K were assumed to be the same as at 173K. The integrated intensities were measured for 5685 reflections from which 4807 independent reflections were observed.

**Table 5.** Crystallographic data and 4-circle neutron data collection details

Diffractometer	5C2 (LLB)
Chemical formula	C <sub>8</sub> H <sub>2</sub> D <sub>4</sub> MnN <sub>8</sub> O
Chemical formula weight	281.09
Space group, cell setting	P2 <sub>1</sub> /c, monoclinic
a (Å)	7.3939(17)
b (Å)	18.858 (4)
c (Å)	8.849(2)
β (degrees)	109.260(4)
Z	4
Monochromator	graphite
Wavelength (Å)	0.833
Crystal size (mm <sup>3</sup> )	9 × 4 × 3.5
Temperature (K)	30 K
Linear absorption coefficient (cm <sup>-1</sup> )	1.134
θ range (degrees)	2.5 < θ < 41.6
Number of measured reflections	5685
Number of independent reflections	4807

No. of used reflections $FN > 3\sigma(FN)$	1731
Number of parameters refined	218
$R(F_N)_{[a]}$	0.042
$R_w(F_N)_{[b]}$	0.039
GOF <sub>[b]</sub>	1.046

[a]  $R(F_N) = (\sum_{hkl} (|F_{No}| - |F_{Nc}|)) / (\sum_{hkl} |F_{No}|)$ . [b]  $R_w(F_N) = [(\sum_{hkl} w(|F_{No}| - |F_{Nc}|)^2) / (\sum_{hkl} w |F_{No}|^2)]^{1/2}$ ,  $w$  weighting scheme (Tukey and Prince) :  $w = (1/\sigma)[1 - (\delta F_N/\sigma)^2]$ . [c] GOF =  $[(\sum_{hkl} w(|F_{No}| - |F_{Nc}|)^2) / (N_o - N_v)]^{1/2}$  with  $N_o$  = number of reflections,  $N_v$  = number of parameters

**Magnetic structures and magnetic phase diagram determination by neutron diffraction.** The same single crystal as the one used for the nuclear structure determination was set on the polarized neutron diffractometer 5C1 at LLB-Orphée with the **c** axis vertical. In order to determine the zero-field antiferromagnetic structures, integrated intensities measurements were performed above and below the magnetic ordering temperature  $T_N = 2.4$  K [3] at 4.3K and 1.5K, respectively. In a second step, a vertical magnetic field (**H** // **c**) was applied to the sample and the peak intensities (up + down) of selected reflections were measured at different temperatures as function of field in order to investigate the magnetic phase diagram. In order to determine the field-induced structure, (**h**, **k**, **l**) integrated intensities were collected at 1.5 K in zero field and above  $H_{c1}$ .

**Flipping ratio measurements by polarized neutron diffraction.** The details of the polarized neutron data collections are reported in Table 6. A first data collection was performed on the polarized neutron diffractometer 5C1 at LLB-Orphée (France) at 5K, in the paramagnetic phase, applying a high vertical magnetic field of 4.5 Tesla (**H** // **c**) to the same sample as above. A set of 212 flipping ratios  $R(hkl)$  was collected for  $-6 < h < 7$ ,  $-10 < k < 15$  and  $0 < l < 3$  leading to 157 reflections after merging the Friedel reflections.

**Table 6.** Polarized neutron data collection details.

Diffractometer	5C1 (LLB)	6T2 (LLB)	
Monochromator	Cu <sub>2</sub> MnAl	Pyrolytic Graphite + polarizing guide	
Wavelength (Å)	0.84	1.4	
Beam polarization	0.88	0.98	
Flipping efficiency	1.000	1.000	
Crystal size (mm <sup>3</sup> )	9x4x3.5	9x4.5x2	
Vertical axis	<b>c</b>	<b>c</b>	
H(Tesla)	4.5	4.5	
T (K)	5	5	10
N measured reflections	212	122	324
N reflections after merging on Friedel (i.e. (h,k,l) and (h,-k,l))	157	98	210
N reflections ( $ 1-R  > 3\sigma$ )	131	54	120

A complementary PND data collection was realized on another single crystal of  $(9 \times 4.5 \times 2)$  mm<sup>3</sup> on the thermal polarized neutron diffractometer 6T2[34], at LLB-Orphée (France), at 5K under an applied field of 4.5T applied along the **c**-axis. Merging the 122 collected flipping ratios  $R(hkl)$

with  $-7 < h < 5$ ,  $-12 < k < 15$  and  $0 < l < 2$  provided a set of 98 reflections including (h,k,l) and (h,-k,l) equivalent reflections. In order to take into account the quality of the nuclear structure determination, only reflections with  $(|F_N^o| > 1.5 \cdot 10^{-12} \text{ cm})$  and those for which a fair agreement between observed  $F_N^o$  and calculated  $F_N^c$  nuclear structure factors, i.e.  $(|F_N^o - F_N^c|/\sigma) < 8$ , were kept in the final flipping ratio data sets. After removing of flipping ratios with extreme values  $R > 2.5$  and  $R < 0.4$ , for which the error bar is systematically underestimated, two sets of 131 and 54 reflections with  $|1-R| > 3\sigma(R)$  were obtained at 5 K for the 5C1 and 6T2 data collections respectively. A third data collection in the paramagnetic phase at a higher temperature (10K) was performed on 6T2, in order to check the influence of short range antiferromagnetic interactions that could affect the spin density determination at 5K, close to the Néel temperature (3K). A total of 324 reflections was measured, leading to 210 reflections after merging on Friedel reflections. Applying the same conditions on  $|F_N^c|$  and  $R_{obs}$  as for the 5K data collections gives a final data set of 120 reflections with  $|1-R| > 3\sigma(R)$ .

## Acknowledgements

Work at EWU was supported by the U.S. National Science Foundation under grant no. 1306158. E.R. thanks for funding the Spanish *Ministerio de Economía y Competitividad* (grant CTQ2015-64579-C3-1-P) and Generalitat de Catalunya for an ICREA Academia award. The computer resources, technical expertise and assistance provided by the Barcelona Supercomputing Centre

**Keywords:** Exchange Coupling • Density Functional Theory, • Transition Metal Compounds • Magnetic Properties • Dicyanamides • Quantum Monte Carlo simulations

- [1] a) T.V. Brinzari, P. Chen, Q.-C. Sun, J. Liu, L.-C. Tung, Y. Wang, J.A. Schlueter, J. Singleton, J.L. Manson, M.-H. Whangbo, A.P. Litvinchuk, J.L. Musfeldt, *Phys. Rev. Lett.* **2013**, *110*, 237202,1-5 and references therein. b) H.N. Bordallo, L.C. Chapon, J.C. Cook, J.R.D. Copley, E. Goremlychkin, S. Kern, S.-H. Lee, T. Yildirim, J.L. Manson, *Appl. Phys. A* **2002**, *74* [Suppl.], S634–S636.
- [2] J.L. Manson, Q. Huang, J.W. Lynn, H.-J. Koo, M.-H. Whangbo, R. Bateman, T. Otsuka, N. Wada, D.N. Argyriou, J. S. Miller, *J. Am. Chem. Soc.* **2001**, *123*, 162-172.
- [3] J.L. Manson, C.M. Brown, Q. Huang, J.A. Schlueter, T. Lancaster, S.J. Blundell, J. Singleton, J.W. Lynn, F.L. Pratt, *Polyhedron* **2013**, *52*, 679–688.
- [4] J.L. Manson, J.A. Schlueter, C.L. Nygren, *Dalton Trans.* **2007**, 646–652.
- [5] a) V. Baron, B. Gillon, A. Cousson, C. Mathonière, O. Kahn, A. Grand, L. Öhrström, B. Delley, M. Bonnet, J.X. Boucherle, *J. Am. Chem. Soc.* **1997**, *119*, 3500-3506. b) V. Baron, B. Gillon, O. Plantevin, A. Cousson, C. Mathonière, O. Kahn, A. Grand, L. Öhrström, B. Delley *J. Am. Chem. Soc.* **1996**, *118*, 11822-11830.
- [6] M. Aebbersold, B. Gillon, O. Plantevin, L. Pardi, O. Kahn, P. Bergerat, I. von Seggern, F. Tuzcek, L. Öhrström, A. Grand, E. Lelièvre-Berna, *J. Am. Chem. Soc.* **1998**, *120*, 5238-5245.
- [7] C. Aronica, E. Jeanneau, H. El Moll, D. Luneau, B. Gillon, A. Goujon, A. Cousson, M. A. Carvajal, V. Robert *Chem. Eur. J.* **2007**, *13*, 3666-3674
- [8] B. Gillon in *MagnetoScience – From Molecules to Materials*, (Eds.: J. Miller, M. Drillon), Wiley-VCH, Weinheim, **2001**, pp. 357-378.
- [9] D. Bordeaux, J. X. Boucherle, B. Delley, B. Gillon, E. Ressouche, J. Schweizer, *Z. Naturforsch.* **1993**, *48a*, 117-119.

- 
- [10] F.M. Romero, R. Ziessel, M. Bonnet, Y. Pontillon, E. Ressouche, J. Schweizer, B. Delley, A. Grand, C. Paulsen, *J. Am. Chem. Soc.* **2000**, *122*, 1298-1309.
- [11] P. W. Betteridge, J. R. Carruthers, R. I. Cooper, K. Prout, D. J. Watkin, *J. Appl. Cryst.* **2003**, *36*, 1487.
- [12] A.C. Larson in *Crystallographic Computing*, (Ed.: F.R. Ahmed, Munksgaard, Copenhagen, **1970**, pp. 291-294 (Eq. 22).
- [13] J.X. Boucherle, B. Gillon, J. Maruani, J. Schweizer, *Mol. Phys.* **1987**, *60*, 1121-1142.
- [14] E. Clementi, D. L. Raimondi, *J. Chem. Phys.* **1963**, *38*, 2686-2689.
- [15] O. Kahn, *Molecular Magnetism*, VCH Publishers, New York, **1993**.
- [16] E. Ruiz, M. Llunell, P. Alemany, *J. Sol. Stat. Chem.* **2003**, *176*, 400-411.
- [17] E. Ruiz, *Struct. Bond.* **2004**, *113*, 71-102.
- [18] E. Ruiz, A. Rodríguez-Fortea, J. Cano, S. Alvarez, P. Alemany, *J. Comp. Chem.* **2003**, *24*, 982-989.
- [19] E. Ruiz, P. Alemany, S. Alvarez, J. Cano, *J. Am. Chem. Soc.* **1997**, *119*, 1297-1303.
- [20] E. Ruiz, J. Cano, S. Alvarez, *Chem. Eur. J.* **2005**, *11*, 4767-4771.
- [21] E. Ruiz, J. Cano, S. Alvarez, A. Caneschi, D. Gatteschi, *J. Am. Chem. Soc.* **2003**, *125*, 6791-6794.
- [22] M. J. Frisch, G. W. Trucks, H. B. Schlegel, G. E. Scuseria, M. A. Robb, J. R. Cheeseman, J. A. Montgomery, T. Vreven, K. N. Kudin, J. C. Burant, J. M. Millam, S. S. Iyengar, J. Tomasi, V. Barone, B. Mennucci, M. Cossi, G. Scalmani, N. Rega, G. A. Petersson, H. Nakatsuji, M. Hada, M. Ehara, K. Toyota, R. Fukuda, J. Hasegawa, H. Ishida, T. Nakajima, Y. Honda, O. Kitao, H. Nakai, M. Klene, X. Li, J. E. Knox, H. P. Hratchian, J. B. Cross, C. Adamo, J. Jaramillo, R. Gomperts, R. E. Stratmann, O. Yazyev, A. J. Austin, R. Cammi, C. Pomelli, J. Ochterski, P. Y. Ayala, K. Morokuma, G. A. Voth, P. Salvador, J. J. Dannenberg, V. G. Zakrzewski, S. Dapprich, A. D. Daniels, M. C. Strain, O. Farkas, D. K. Malick, A. D. Rabuck, K. Raghavachari, J. B. Foresman, J. V. Ortiz, Q. Cui, A. G. Baboul, S. Clifford, J. Cioslowski, B. B. Stefanov, G. Liu, A. Liashenko, P. Piskorz, I. Komaromi, R. L. Martin, D. J. Fox, T. Keith, M. A. Al-Laham, C. Y. Peng, A. Nanayakkara, M. Challacombe, P. M. W. Gill, B. Johnson, W. Chen, M. W. Wong, C. Gonzalez, and J. A. Pople, Gaussian 03 (Revision C.2); Gaussian, Inc: Pittsburgh, PA, **2003**.
- [23] A. D. Becke, *J. Chem. Phys.* **1993**, *98*, 5648-5652.
- [24] A. Schaefer, C. Huber, R. Ahlrichs, *J. Chem. Phys.* **1994**, *100*, 5829-5835.
- [25] A. Schaefer, H. Horn, R. Ahlrichs, *J. Chem. Phys.* **1992**, *97*, 2571-2577.
- [26] Jaguar 6.0; Schrödinger, Inc.: Portland, **2005**.
- [27] V. Blum, V. R. Gehrke, F. Hanke, P. Havu, V. Havu, X. Ren, K. Reuter, M. Scheffler, *Comput. Phys. Commun.* **2009**, *180*, 2175-2196.
- [28] D. Aravena, D. Venegas-Yazigi, E. Ruiz, *Sci. Rep.* **2016**, *6*, 23847.
- [29] B. Doistau, L. Benda, J.-L. Cantin, L.-M. Chamoreau, E. Ruiz, V. Marvaud, B. Hasenknopf, G. Vives *Journal of the American Chemical Society* **2017**, *139*, 9213-9220.
- [30] A.W. Sandvik, *Phys. Rev. B* **1999**, *59*, 14157.
- [31] B. Bauer, L.D. Carr, H.G. Evertz, A. Feiguin, J. Freire, S. Fuchs, L. Gamper, J. Gukelberger, E. Gull, S. Guertler, A. Hehn, R. Igarashi, S.V. Isakov, D. Koop, P.N. Ma, P. Mates, H. Matsuo, O. Parcollet, G. Pawłowski, J.D. Picon, L. Pollet, E. Santos, V.W. Scarola, U. Schollwöck, C. Silva, B. Surer, S. Todo, S. Trebst, M. Troyer, M.L. Wall, P. Werner, S. Wessel, *J. Stat. Mech. Theor. Exp.* **2011**, 2011, P05001.
- [32] J. Cano, E. Ruiz, S. Alvarez, M. Verdaguier, *Comments on Inorg. Chem.* **1998**, *20*, 27-56.
- [33] E. Ruiz, J. Cirera, S. Alvarez, *Coord. Chem. Rev.* **2005**, *249*, 2649-2660.
- [34] A. Gukasov, A. Goujon, J.-L. Meuriot, C. Person, G. Exil, G. Koskas, *Physica B: Condensed Matter* **2007**, *397*, 131-134.
-

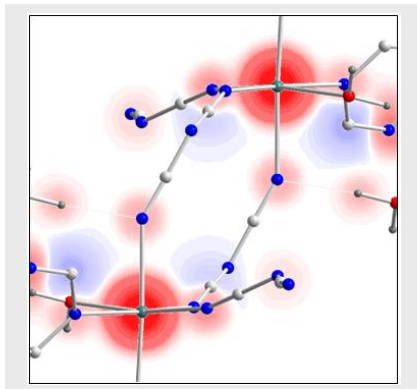
---

## Entry for the Table of Contents

### FULL PAPER

---

The magnetic phase diagram of the quasi bidimensional  $\text{Mn(dca)}_2(\text{pym})(\text{H}_2\text{O})$  compound was established by neutron diffraction. The magnetic interaction pathways are visualized by the induced spin distribution from polarised neutron diffraction (PND) in the paramagnetic phase. Antiferromagnetic coupling is mediated by the dca bridges inside the layers and by H-bonding between the layers. DFT and QMC calculations are confronted with the PND results and SQUID susceptibility measurements



#### **Role of H-bonding in magnetic ordering of a quasi-2D Mn-dca polymer**

*B. Gillon\**, *A. Hammerschmied*,  
*A. Gukasov*, *A. Cousson*, *T. Cauchy*, *E. Ruiz*, *J.A. Schlueter* and *J.L. Manson\**

**Page No. – Page No.**

**H-mediated magnetic interactions between layers in a two-dimensional Mn-dca polymer : Neutron Diffraction, DFT and Quantum Monte Carlo calculations**